Journal of Alloys and Compounds 510 (2012) 15–25

Contents lists available at SciVerse ScienceDirect

Journal of Alloys and Compounds

journal homepage: www.elsevier.com/locate/jallcom

# Study on edge cracking and texture evolution during 150 °C rolling of magnesium alloys: The effects of axial ratio and grain size

M. Pekguleryuz[a,*], M. Celikin[a], M. Hoseini[a], A. Becerra[b,1], L. Mackenzie[c,1]

[a] McGill University, Montreal, QC, Canada
[b] Hatch Associates, Montreal, QC, Canada
[c] Novelis Inc., Kingston, ON, Canada

ARTICLE INFO

*Article history:*
Received 17 May 2011
Received in revised form 28 August 2011
Accepted 29 August 2011
Available online 8 September 2011

*Keywords:*
Magnesium
Lithium
Indium
Zinc
Lattice parameters
Grain size
Texture

ABSTRACT

Pure Mg, AZ31 (Mg–3 wt%Al–1 wt%Zn) and experimental alloys, Mg–1 wt%Zn–1 wt%In, Mg–2 wt%Li–1 wt%Zn, Mg–2 wt%Li–1 wt%Zn–1 wt%In were rolled at 150 °C to 0.3 and 0.55 strain. The samples rolled to 0.3 strain were subsequently annealed for 10 min at 400 °C. The texture was evaluated in rolled and in rolled/annealed conditions. The axial ratio ($c/a$) of the alloys strongly influenced edge cracking during rolling (expressed as cracking index, $I_C$), which was explained via the influence of $c/a$ on the twinning mode. The as-cast grain size did not correlate to $I_C$ (edge cracking). Texture intensity was strongly influenced by the as-cast grain size (which was attributed to plastic compatibility at grain boundaries), showed weak correlation to the lattice parameter $a$, but did not depend on $c/a$. The Mg–2 wt%Li–1 wt%Zn alloy, with fine grain size and small $c/a$ and $a$, exhibited the optimum combination of weak texture and crack-free rolling at 150 °C.

© 2011 Elsevier B.V. All rights reserved.

## 1. Introduction

The interest of automotive companies in weight reduction has led to new research in wrought Mg alloys. Sheet formability is currently the main interest since sheet metal parts make up about 25% of the vehicle mass [1]. The replacement of the heavier sheet products with the light weight magnesium would result in a significant weight reduction and in turn less fuel consumption [1].

Studies conducted on the deformation behavior of Mg and on new processing alternatives for Mg sheet [1–14] have shown the potential of forming at elevated temperatures and of superplastic forming. Equal-channel angular extrusion (ECAE) which results in extreme refinement of grain size can also be viably used for Mg sheet production. Currently, AZ31 (Mg–3Al–1Zn) is the most common Mg sheet alloy. It, however, suffers from edge-cracking during rolling, as well as a basal texture, a non-homogeneous recrystallized grain-size or partial recrystallization leading to limited room temperature formability. Improving the room-temperature formability of Mg is challenging and would require alloying or processing to alter the textures and the recrystallization behavior. Recently, it has been shown that [15,16] twin-roll-cast (TRC) AZ31 sheet can develop weaker textures upon annealing due to the metastable cast/deformed structure that develops in TRC. New alloys are also being investigated to weaken the Mg sheet texture during rolling and annealing [17–22].

It is not yet clearly known which parameters or features of Mg alloys influence its forming or deformation behavior. The grain size of the cast structure may have an effect on the subsequent processing and deformation behavior. An area not much discussed is the effect of lattice parameters and the axial ratio ($c/a$) of the hexagonal-closed packed (HCP) crystal on the deformation and the rolling behavior. Previous research by Becerra et al. [23,24] has shown that lithium (Li) and indium (In) change the axial ratio of Mg, and that zinc (Zn) additions decrease the grain size, $D$. This paper reports on partial results of an ongoing study investigating the effects of solute elements on Mg sheet. As such, the present paper focuses on the effects of combined additions of Li, In and Zn on the rolling at 150 °C and on subsequent annealing of magnesium in comparison to the commercial sheet alloy AZ31.

## 2. Background

The engineering parameter commonly termed “workability” (forgeability, rollability, extrudability and formability) refers to the ease with which a material can be shaped by plastic deformation without the onset of fracture; it is influenced not only by microstructure, temperature, strain rate and strain but also

* Corresponding author. Tel.: +1 514 398 1528; fax: +1 514 398 4492.
*E-mail address:* mihriban.pekguleryuz@mcgill.ca (M. Pekguleryuz).
[1] Formerly with McGill University.

0925-8388/$ – see front matter © 2011 Elsevier B.V. All rights reserved.
doi:10.1016/j.jallcom.2011.08.093

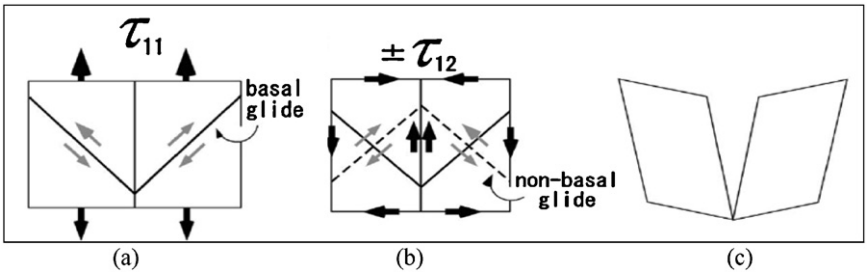


**Fig. 1.** Schematic drawing showing two crystals (a) before deformation, (b) state of stress to maintain contact between two grains along a grain boundary. (c) Deformed condition without bonding along the grain boundary [14].

by the state-of-stress in the deformation zone. *Intrinsic workability* depends on microstructure and prior processing history of the material and is embedded in the flow stress variation with temperature, strain rate and strain, and is represented mathematically by constitutive equations [25]. However, certain microstructural changes also occur in the material as response to parameters, such as dynamic recrystallization (DRX), superplastic deformation, dynamic recovery (DRV), twinning, edge-cracking, Luder's or kink bands, wedge cracking (crack at triple junctions of grains during grain boundary sliding), void formation (at particle/matrix interface or inside particles), intercrystalline cracking (grain-boundary cracking due to incipient melting), flow instability (shear band formation) and flow localization (localized wavy shear bands). While DRX and superplastic deformation are "safe" mechanisms for hot-deformation, and DRV is safe for warm working; all other mechanisms are problematic and need to be avoided [26]. In this study edge cracking during rolling is investigated which is one of the detrimental mechanisms seen during 150 °C rolling of Mg alloys.

### 2.1. The effects of axial ratio and of lattice parameters on deformation

It is generally known that cubic metals with body-centered and face-centered cubic structures (BCC and FCC) are more formable than HCP metals such as Mg since they can provide at least five (5) independent slip systems required by the von Mises criterion for formability. HCP Mg has only two (2) independent slip systems at room temperature leading to limited formability. However, the axial ratio differs in different HCP metals, which affects the deformation of HCP metals [27,28]. The lattice parameters of HCP Mg give a $c/a$ of 1.62354 at 25 °C, which, as in Cd and Zn, results in low critical resolved shear stress (CRSS) on the basal {0 0 0 1} plane favoring basal slip. Ti, on the other hand, has much lower $c/a$ than Mg, Cd, and Zn; it has high basal CRSS but low prismatic CRSS, and exhibits non-basal slip at room temperature and, consequently, improved formability; this means that as $c/a$ decreases towards 1.59 (as in Ti), CRSS for basal slip increases in HCP crystals and other HCP slip systems (prismatic and/or pyramidal slip systems) are activated (Tables 1 and 2).

Temperature and deformation cause changes in lattice spacing. The temperature effect may be due not only to thermal expansion but also to electron overlap to the second Brillouin zone [23] causing a change in $c/a$. The improved formability of Mg above 250 °C is related to the onset of electron overlap for Mg as well as to thermal expansion. Stohr et al. [29] have seen that temperature has a strong effect on pyramidal slip and $\langle c+a\rangle$ dislocations. It is also known that tensile stress in the $c$-direction may cause an increase in the $c$-spacing [28]. In this study, rolling was conducted at 150 °C where no significant non-basal slip due to thermal activation would be expected.

Certain solutes can also change the lattice parameters and the axial ratio of HCP Mg and affect formability. Li in solid solution is known to reduce the $c/a$ in the α-phase from 1.624 to 1.61 and to reduce the CRSS on the prismatic slip system [28]. Texture modeling and transmission electron microscopy (TEM) studies indicate that Li also increases the glide of $\langle c+a\rangle$ dislocations on pyramidal planes in HCP α-Mg, where the role of Li is related [29–31] to the stability of partials dissociated from the $\langle c+a\rangle$ dislocations. This is considered to provide additional slip modes to satisfy the von Mises criterion, which may partly explain the increase in formability associated with low levels of Li additions. The lattice parameters of Mg solid solution alloys with Li, In and/or Zn additions have been determined via X-ray diffraction (XRD) by Becerra et al. [23]. Li decreased the axial ratio ($c/a$) of magnesium from 1.6424 to 1.6068 within 0–16 at%Li. Indium increases the $c/a$ of Mg to 1.6261 as indium is increased from 2.8 at% towards 3.3 at% while Zn showed no effect on $c/a$ in the 0.2–0.7 at% range. The effects were explained by electron overlap through the first Brillouin zone and by Vegard's Law. Notably, the $c/a$ versus %In curve goes through a reversal and In decreases the $c/a$ between 2.2 and 2.8 at%In.

The change in the deformation mechanism due to reduced axial ratio can be attributed to the change in the interplanar spacing, $d$, since the shear stress required to move dislocations is given by the Peierls stress,

$$\tau_p = Pe^{\{-2\pi d/[b(1-\mu)]\}}, \tag{1}$$

where $P$ is a factor depending on the shear modulus and Poisson's ratio, $\mu$; $b$ is the magnitude of the Burgers vector of the dislocation, and $d$ is the interplanar spacing. The critical resolved shear stress, $\tau_{CRSS}$, is related to the Peierls stresses, $\tau_p$. In a recent study, Uesugi et al. [5] have calculated $\tau_p$ from first principles as

$$\tau_p = \frac{Kb}{a'}\exp\left(-\frac{Kb}{2a'\tau_{max}}\right), \tag{2}$$

**Table 1**
Basal CRSS and $c/a$ for HCP metals (25 °C).

| Metal | CRSS (psi) | $c/a$ |
|---|---|---|
| Cd | 82 | 1.886 |
| Mg | 63 | 1.624 |
| Zn | 26 | 1.856 |
| Ti | 16,000 | 1.588 |
| Be | 5,700 | 1.586 |

**Table 2**
Slip systems in magnesium.

| Slip system | Slip direction | Slip plane and direction | Independent slip systems |
|---|---|---|---|
| Basal | $a$ | {0 0 0 1} ⟨1 1 $\bar{2}$ 0⟩ | 2 |
| Prismatic | $a$ | {1 0 $\bar{1}$ 0} ⟨1 1 $\bar{2}$ 0⟩ | 2 |
| Pyramidal type I | $a$ | {1 0 $\bar{1}$ 1} ⟨1 1 $\bar{2}$ 0⟩ | 4 |
| Pyramidal type II | $c+a$ | {1 1 $\bar{2}$ 2} ⟨1 1 $\bar{2}$ 3⟩ | 5 |

where

$K$ = energy factor (depends on elastic constants and the type of dislocation),
$a'$ = interplanar spacing in the direction of dislocation sliding on slip plane ($a' = a/2$ for basal slip where $a$ is the lattice parameter and $a' = a$ for prismatic plane),
$b$ = Burgers vector; $b = (a/3)^{1/2}$ for Shockley partial dislocations of the basal plane and $b = a$ for edge dislocations of the prismatic plane,
$\tau_{max}$ = max. restoring force (=max. slope of the generalized stacking fault energy in the analysis).

They have shown [5] that the difference in the CRSS of basal and prismatic slip can be explained by the differences in the Peierls stresses of the basal $\langle a \rangle$ and of the prismatic $\langle a \rangle$ dislocations (4 MPa vs. 118 MPa). Eq. (2) interestingly indicates that changing the $a$-spacing would not influence the Peierls stresses and the CRSS for prismatic slip (because $b = 2a$ for edge dislocations), but it would alter the basal slip of partial dislocations because their $b = (a/3)^{1/2}$. Research [23] has shown that a large decrease in $a$ occurs with solute additions of In > 0.2 at% and Zn > 0.2 at%. The study also reveals that $c/a$ would substantially decrease at a composition range between 2.2 and 2.8 at%In, where non-basal slip of whole dislocations could be facilitated [23]. A decrease in the $a$-parameter points towards a possible ease in the cross-slip of basal partials.

### 2.2. Grain size and plastic compatibility

It has been determined that grain size and grain structure influence deformation behavior [4–7]. Twinning becomes difficult with decreasing grain size [32]. It has been found that [33] elongation-to-failure increased up to 15% when grain size was reduced from 400 to 17 μm.

Koike et al. [14] have shown that the activity of non-basal slip can depend on grain-size dependent compatibility stresses at grain boundaries. The activation of the secondary slip systems by plastic compatibility stress has been well-established by previous studies. In the case of Mg, plastic heterogeneity is very strong and may give rise to a large plastic compatibility stress [14] at the grain boundaries. Fig. 1a schematically illustrates how two grains with basal planes oriented 45° to the tensile axis and tilted 90° across the grain boundary would require (plastic compatibility) shear stresses (Fig. 1b) to activate non-basal slip to remain bonded at the grain boundary, because otherwise (if only basal slip were operative) the grains would assume oval shape (Fig. 1c) and fracture would occur along grain boundaries. Under compressive loading, the direction of the stresses would change, but the effect would be similar. This suggests that the basal slip systems cannot operate near grain boundaries unless the non-basal glide systems become active. Koike et al. [14] have shown that cross-slipping of $\langle a \rangle$ dislocations to non-basal planes was significantly active as a result of grain-boundary compatibility stresses and that dynamic recovery took place in AZ31B alloy at 2% strain. As they explain, when the grain size decreases, twinning becomes difficult, but plastic-compatibility stresses at the grain boundaries assume importance. In Ti–Mn alloys, the average length of the secondary slip lines adjacent to grain boundaries is reported [34] to be ~10 μm, regardless of grain size in the range 49–94 μm. Koike et al. [14] consider that this deformation mechanism is not limited to the ECAE-processed Mg alloys but is also applicable to other fine-grained Mg alloys. It can be expected that the degree of the non-basal activity would depend on grain size in most Mg alloys. Koike et al. [14] have also seen that at higher strain (16%), AZ31 did show twinning (despite the fine grain size) which led to work softening at room temperature.

Although processing conditions and inoculation can alter the grain size, the intrinsic grain refining ability of the alloy can also be important. This is especially important in twin-roll-casting where the process can result in a surface region of columnar grains (in addition to fine equiaxed grains in the center) [15,16], the extent of which would depend on the intrinsic grain refining of the alloy. The prediction of grain size from solute content has been under investigation for some time [35]. Becerra et al. [24] have studied multi-component solid-solution alloys of Mg with Li, In and Zn and reported that they exhibit low $c/a$ and fine grain size.

### 2.3. Texture in magnesium alloy sheet

Rolling tends to orient the basal planes approximately parallel to the surface with the $[1\,0\,\bar{1}\,0]$ diagonal axis in the rolling direction. Kaiser et al. [36] have studied the AZ31 H-24 structure and saw that the sheet exhibited a heterogeneous grain-size distribution with a mixture of large and small grains. While the average grain size was 20 μm, there were grains as large 60 μm. The typical texture of an egg-shaped distribution of $\{0\,0\,0\,1\}$ planes was also seen. Double textures occur in rolled Mg with the two poles inclined 10–40° (i.e. greater scatter in the longitudinal direction) causing higher properties in the transverse direction of the sheet. The scatter in the basal planes has been attributed to the formation of kink bands or deformation bands during rolling [28,36]. On the surface, basal normals are perpendicular to the rolling plane yielding a single texture but deviate up to 15° as one moves deeper into the sheet giving double textures. Directionality can vary considerably with depth below the surface and may differ in different alloys. The resolved shear stress of the basal plane of HCP crystals is dependent on the orientation of the plane with respect to the stress axis. The deformation of magnesium at room temperature is, therefore, dependent on plastic anisotropy. It has been observed that a smaller grain size is needed to avoid texture and to increase random orientation [36]. Mackenzie et al. [18] studied the effects of processing parameters (rolling temperature, annealing) on Mg–1 wt%Li alloy. Rolling textures were basal with the basal poles split and rotated towards the rolling direction. Annealing was seen to result in a single peak of basal poles replacing the "split" rolling texture.

Non-basal textures, though rare, have been found in certain Mg alloy systems [17,37–41]. Non-basal textures in the WE-series (yttrium-rare earth) of magnesium alloys have been associated with recrystallization and grain growth [37–39]. In Mg–Zn–Ce alloys [18], it was found that the recrystallization texture was non-basal with the basal poles orientated ~45° away from the normal direction towards the transverse direction.

### 2.4. Edge cracking and twinning during sheet rolling of magnesium alloys

Edge cracking is usually attributed to a form of directionality termed compression banding, which is a result of twinning in rolled sheet that has undergone compression [42]. Compression bands appear to be responsible for edge cracking in finish rolling of AZ31 alloy sheet. Basal planes become oriented parallel to the band plane and, hence, compression bands become favorable sites for basal slip to occur, leading to eventual cracking.

It is known that the twinning shear is related to the axial ratio in HCP crystals [43–45] as presented in Fig. 2 where the twinning systems with positive slope indicate compression (contraction) twins and those with negative slopes indicate tension (extension) twins along the $c$-axis. Fig. 2 also presents the axial ratios of the HCP metals and the most common twinning modes activated in them. Within the range of the axial ratios of the HCP metals (1.568–1.886), the $\{1\,0\,\bar{1}\,2\}$ $\langle \bar{1}\,0\,1\,1 \rangle$ the shear direction reverses at an axial ratio of $\sqrt{3}$, where this twinning mode becomes compressive for Zn and Cd,

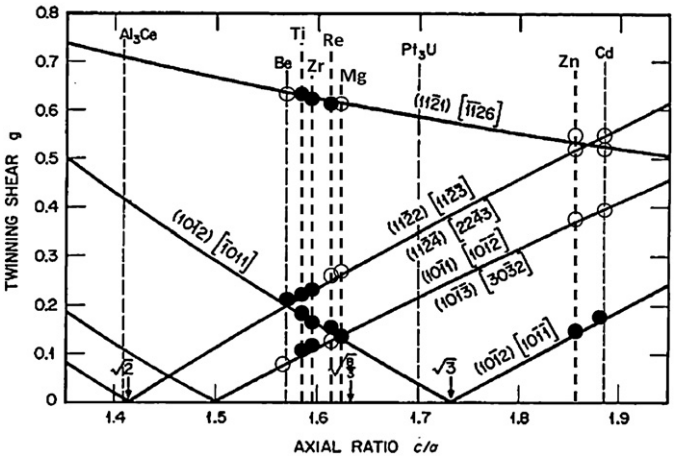


**Fig. 2.** Twinning shear versus axial ratio. For the seven HCP metals, the filled symbols indicate that the twin mode is active [43,44].

but is tensile for all other HCP metals (Be, Ti, Zr, Re, Mg). HCP metals that exhibit high ductility (Re, Zr, Ti) twin profusely in both tensile and compressive modes and those that are very brittle (Be, Zn) twin only by the most common type $\{1\,0\,\bar{1}\,2\}$ tension twin [43]. In Mg, the $\{1\,0\,\bar{1}\,2\}$ tension twins are followed by $\{1\,0\,\bar{1}\,1\}$ compression twins. Generally, the lower the value of twinning shear of a given twin mode, the higher is the frequency of its occurrence. This correlation has been generally observed as indicated by Fig. 2 and also by those experiments in which the axial ratio was changed by alloying [43]; the additional factors are the ease with which atomic shuffling can occur to nucleate the twin and the ease of gliding parameters. The absence of $(1\,0\,\bar{1}\,1)$ $(1\,0\,\bar{1}\,2)$ compression twins in Be despite the low twinning shear is related to the complex atom shuffling, while the occurrence of $\{1\,1\,2\,1\}$ 1/3 $(1\,1\,2\,6)$ twinning in Ti, Zr, and Re in spite of its relatively large twinning shear is attributed to the relatively simple atomic shuffling [43]. It is, therefore, possible to influence the twinning behavior of Mg alloys via changes in the axial ratio.

The objective of this study was to investigate the combined effects of axial ratio and grain size of Mg through alloying with Li, Zn, and In on the edge cracking behavior and texture. Lithium and indium were selected due their known effect on $c/a$ [21] and zinc is selected because of its grain refining effect [24]. This work is part of an ongoing study to develop magnesium sheet alloys with weak or random texture in order to provide formable lightweight automotive sheet based on Mg.

## 3. Experimental procedure

A number of solid solution magnesium alloys was synthesized using Mg, Zn, Li, and In. The alloys were prepared from pure metals: magnesium (99.98 wt%) was supplied by Timminco Metals (now Applied Magnesium); pure lithium (99.98 wt%) and indium (99.999 wt%) were purchased from Alfa Aeser. The alloys were made by adding the elements to pure magnesium melt in a Lindberg electric resistance furnace at 680 °C, under $CO_2$–0.5%$SF_6$ gas cover, except for the Li-containing alloys which were prepared under argon. AZ31 was obtained from Timminco.

The alloys were cast into a steel permanent mold to produce plates with the dimensions of 2.7 cm × 10.2 cm × 2.5 cm. The internal surface of the mold was sprayed with a boron-nitride coating supplied by Pyrotek. The mold was preheated to 425 °C. The castings were homogenized for sixteen (16) hours under argon at 400 °C to eliminate microsegregation. The chemical compositions were determined via Inductively-Coupled Plasma Atomic-Emission Spectroscopy (ICP-AES) at Genitest Inc (Montreal). The compositions of the alloys are shown in Table 3; the alloy compositions in the text are referred to in wt% unless otherwise indicated.

Rolling specimens had dimensions of 6 mm × 25 mm × 25 mm and were removed from cast plates (Fig. 3). All alloys were rolled at 150 °C using the McGill University Stanat rolling machine. The specimens were preheated for 15 min at 150 °C prior the first rolling pass, and reheated for 5 min in between passes. One set of specimens was rolled in 7 passes to an engineering strain of 0.30. A second set of specimens was rolled in 15 passes to an engineering strain of 0.55. Following rolling, specimens were quenched in water. Rolled (7 passes) and recrystallized microstructures and textures were analyzed to assess the potential for subsequent formability. Edge cracking, after 0.55 strain at 150 °C, was used to rank the alloys visually. An index system from 1 to 5 was used where 1 showed minimum cracking and 5 indicated severe cracking. Specimens rolled in 7 passes to 0.3 strain were annealed for 10 min at 400 °C.

**Table 3**
Compositions of magnesium alloys (at%).

| Alloy (at%) | Alloy (wt%) |
|---|---|
| Mg | Mg |
| Mg–0.35Zn | Mg–0.87Zn |
| Mg–6.2Li–0.34Zn | Mg–1.84Li–0.95Zn |
| Mg–0.35Zn–0.19In | Mg–0.93Zn–0.88In |
| Mg–6.2Li–0.36Zn–0.2In | Mg–6.2Li–0.36Zn–0.2In |
| Mg–2.43Al–0.34Zn | Mg–2.68Al–0.89Zn |

The sheet specimens were mechanically ground to the mid-plane with SiC paper and polished with diamond paste for texture analysis and etched for 60 s in 10% nital (10 ml nitric acid, 90 ml ethanol) at room temperature in order to remove surface strain. X-ray texture analysis was performed using a Siemens D-500 diffractometer. Incomplete (0 0 0 2), and pole figures were recorded, and the orientation distribution function (ODF) was constructed using TexTools texture analysis software. In the cases of X-ray texture analysis, the pole figure contour lines have been given values of 1$x$, 2$x$, 3$x$, 4$x$. . . random, or in some cases values of 1$x$, 1.25$x$, 1.5$x$, 1.75$x$. . . random. Values were selected, as appropriate, in order to highlight significant orientation characteristics, and have been indicated in each pole figure.

Microstructures were analyzed using Epiphot 200 Nikon microscope. Grain size measurements were carried on etched samples. Either 5% nital or acetic-picric etchant was used to reveal grain boundaries. An Olympus SZ 40 stereoscope and an Epiphot 200 Nikon microscope and the mean linear intercept (MLI) method were used to determine grain size. A Philips CM200 TEM was used at 200 kV to study the twining types. The TEM samples were cut from rolled specimens to obtain 1.0 mm plates by slow speed diamond saw and prepared by mechanically polishing down to 0.1 mm thickness, which were punched to obtain 3.0 mm dia. discs and double jet polished at −30 °C in a solution of 3% nital at 20 V.

## 4. Results and discussion

### 4.1. As-cast grain size

As-cast grain size depends on alloy characteristics and processing and can be an important factor governing the subsequent deformation. The as-cast grain sizes of the rolling samples are shown in Fig. 4. It is noted that pure Mg as well as certain alloys and especially Mg–1Zn and Mg–1Zn–1In exhibit a mixture of columnar and equiaxed grains. The fraction of equiaxed grains ($f_e$) was determined on the macrographs. An effective as-cast grain size

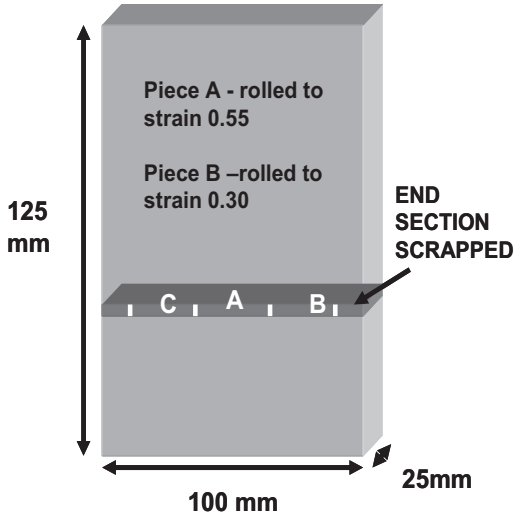


**Fig. 3.** Schematic showing location of the slice and extracted from the thick block and of the rolling specimens (6 mm × 25 mm × 25 mm) A and C that were removed from the slice.

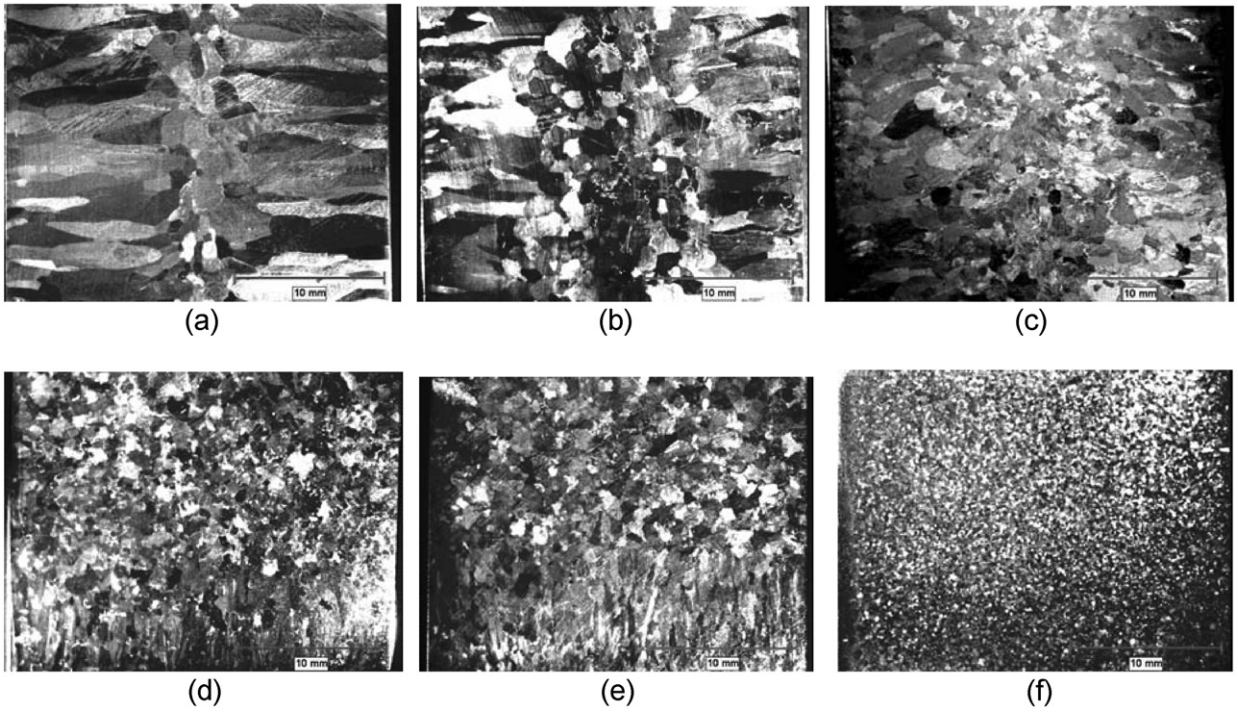


**Fig. 4.** Grain structures of rolling samples (a) pure Mg; (b) Mg–0.35Zn; (c) Mg–0.35Zn–0.19In; (d) Mg–6.2Li–0.34Zn; (e) Mg–6.2Li–0.36Zn–0.2In; (f) AZ31 (scale bar = 10 mm).

was assigned to the as-cast samples taking into account the mixed mode of the grain structure as well as the grain size (Table 4). The following equation was used to assign the effective grain size, $D'$

$$D' = [f_c(D_c) + f_e(d_e)] \quad (3)$$

where

$f_c$ = area fraction of columnar grains;
$D_c$ = average diameter of columnar grains = $(D_{minor} + D_{major})/2$;
$f_e$ = area fraction of equiaxed grains; and
$D_e$ = average grain size of equiaxed grains.

### 4.2. Lab-scale rolling and edge cracking

The specimens rolled to 15 passes are shown in Fig. 5a. As a reference, the commercial magnesium sheet alloy AZ31 (Mg–3Al–1Zn) was also cast and rolled under the same conditions. As seen in Fig. 5a and b, the AZ31 alloy showed severe edge cracking while the Li-containing alloys were crack-free and the other alloys (Mg–Zn and Mg–Zn–In) showed light-to-moderate cracking (Fig. 5c and d). The AZ31 alloy in this study did exhibit crack-free rolling up to 7 passes (0.3 strain), but cracked severely with further deformation. The edge cracking indices ($I_C$) of the experimental alloys ranged from 1 to 3 (Table 4). Pure Mg had large edge cracks and was assigned an $I_C$ of 4 while the AZ31 alloy was assigned an $I_C$ of 5 due to the severe edge cracking.

#### 4.2.1. The effect of lattice parameters

Plotting $I_C$ versus $c/a$ and the effective grain size, $D'$, shows that $c/a$ exerts an important effect on edge cracking (Fig. 6a). This is an unexpected result where an effect of the axial ratio on edge cracking has not been previously reported. Edge cracking index versus $c/a$ can be expressed as

$$I_C \sim 550(c/a) - 880 \quad \text{with} \quad R^2 = 0.85. \quad (4)$$

The $a$-parameters of the alloys (Table 4) suggest that, when AZ31 is excluded, the edge cracking index does have strong dependence ($R^2$ = 0.96) on the $a$-parameter of the experimental alloys (Fig. 6b):

$$I_C = 316(a) - 1010 \quad (5)$$

Notably, the Burgers vector of Shockley partials varies (Eq. (2)) with the $a$-parameter as $b = (a/3)^{1/2}$; as $a$ decreases so does $b$ for partial dislocations and cross-slip is promoted. AZ31 despite having the lowest $a$-parameter falls outside this relationship. This suggests that while the $c/a$ and $a$ do have influence on edge cracking, the effect could be indirect or overshadowed by other mechanisms such as twinning.

**Table 4**
Axial ratio, grain structure and size, edge cracking index and texture intensity.

| Alloy, at% | $a$ | $c/a$ | Grain structure: %columnar ($D_c$)[a] + % equiaxed ($D$) | Effective cast grain size, $D'$, mm | Re-crystallized grain size, $d$ | Edge cracking index | Maximum intensity | |
|---|---|---|---|---|---|---|---|---|
| | | | | | | | Rolled | Rolled + annealed |
| Mg | 3.2088 | 1.6240 | 84% col (6500 μm) + 16% eq (1000 μm) | 6.1 | 46 | High/4 | 12.2 | 17.9 |
| Mg–0.35Zn | – | 1.6240 | 60% col (3500 μm) + 40% eq (1500 μm) | 2.7 | – | Moderate/3 | – | – |
| Mg–0.35Zn–0.19In | 3.2069 | 1.6241 | 40% col (2700 μm) + 60% eq (2000 μm) | 2.3 | 40 | Moderate/3 | 5.4 | 4.9 |
| Mg–6.2Li–0.34Zn | 3.2009 | 1.6190 | 100% equiaxed (1800 μm) | 1.8 | 48 | Minimum/1 | 4.2 | 2.6 |
| Mg–6.2Li–0.36Zn–0.2In | 3.1991 | 1.6190 | 100% equiaxed (1000 μm) | 1.0 | 49 | Minimum/1 | 6.2 | 3.0 |
| AZ31 | 3.1993 | 1.6247 | 100% equiaxed 150 μm | 0.15 | 51 | Severe/5 | 3.4 | 2.4 |

[a] $D_c$ = ave. diameter of columnar grains = $(D_{minor} + D_{major})/2$; $D$ = ave. grain diameter of equiaxed region.

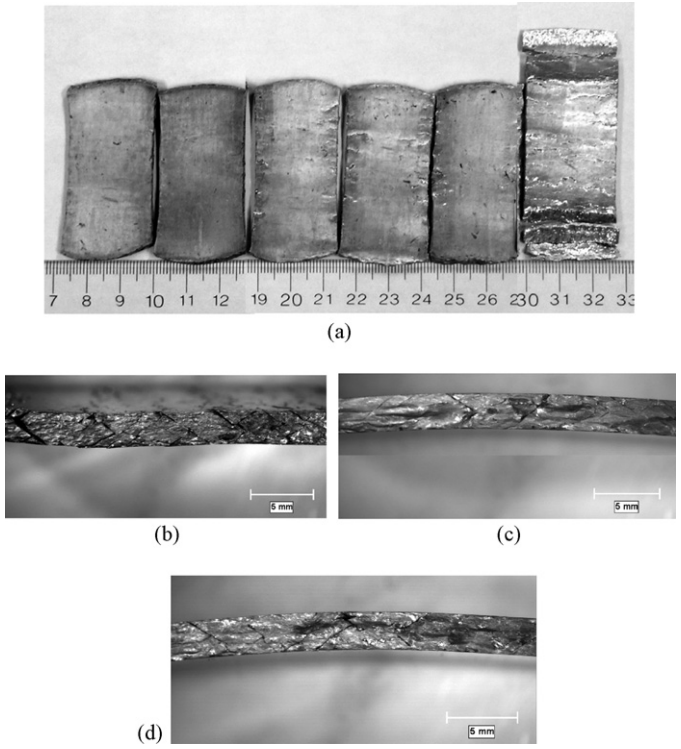


**Fig. 5.** (a) Alloys rolled 15 passes at 150 °C (from left to right: for Mg–Li–Zn, Mg–Li–Zn–In, Mg–Zn–In, Mg–Zn, Mg and AZ31). Edge cracks after 15 passes in (b) AZ31, (c) Mg–Li–Zn–In, (d) Mg–Li–Zn.

### 4.2.2. The effect of grain size

The effective grain size correlates with edge cracking in the experimental alloys as

$$I_C = 0.6D' + 0.8, \quad (6)$$

however, the relationship is not very strong ($R^2 = 0.71$) and it does not explain the edge-cracking behavior of AZ31 (Fig. 6c). Despite the very fine grain size, AZ31 shows severe edge cracking after 15 passes. The rolling trials have shown that at 7 passes (0.3 strain) the AZ31 is free from edge-cracking, but starts to exhibit severe cracking with further rolling towards 0.55 strain. This agrees with Koike's findings [14] where fine grained AZ31 shows no twinning at 2% strain, but twinning and work softening inside the twins are seen at 16% strain under tensile loading. It is again interesting to note that the ductility during rolling is not related to the initial grain-size of the starting material.

### 4.2.3. The role of twinning

Two alloys were selected to investigate if twinning modes can explain the edge cracking behavior during rolling at 150 °C: (i) AZ31 which showed severe edge cracking and (ii) Mg–Li–Zn alloy which did not. TEM analyses were conducted to investigate the twinning modes in the alloys.

*Mg–Li–Zn*: Fig. 7 shows the TEM image of a twin in the Mg–Li–Zn alloy rolled 15 passes at 150 °C, together with the diffraction patterns obtained from the twin and the matrix. The rotation angles, $\alpha$, of specimens during imaging of the diffraction patterns were $\alpha_{mat} = -3.42°$ and $\alpha_{twin} = 16.91°$. Based on the diffraction patterns, it is determined that the zone axes ($B$) are $B_{Mat} = [1\,\bar{2}\,1\,\bar{3}]$ and $B_{twin} = [\bar{1}\,2\,\bar{1}\,6]$ for the matrix and the twin, respectively. The planes corresponding to these zones are $P_{mat} = (1\,\bar{2}\,1\,\bar{5}.27)$ and $P_{twin} = (\bar{1}\,2\,\bar{1}\,10.53)$. The angle between the two planes calculated using equation given in [46] is $\varphi = 165.6° = (180 - \theta)$. Thus, for $\theta = 14.4$, the twin misorientation

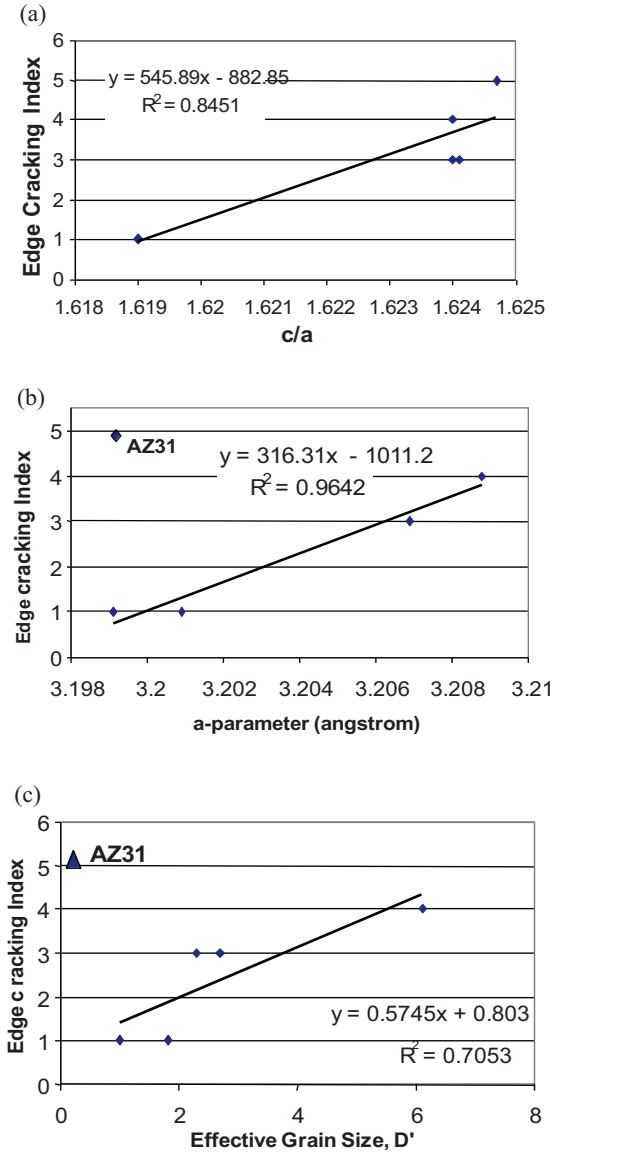


**Fig. 6.** Edge cracking index versus (a) $c/a$, (b) $a$ parameter, and (c) effective grain size.

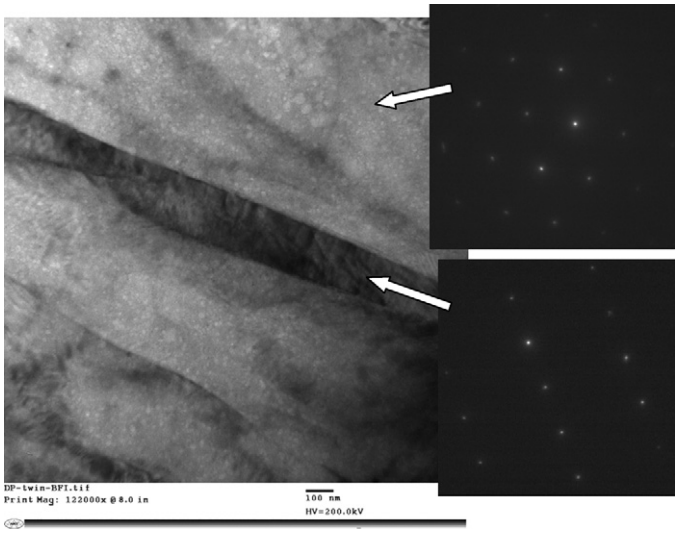


**Fig. 7.** TEM image of a twin in Mg–Li–Zn matrix following 15 passes of rolling at 150 °C.

**Table 5**
Possible boundary misorientation axis and angles for different twin types and double twins in magnesium [46].

| Twin type | Angle and axis of misorientation |
|---|---|
| $\{1\,0\,\bar{1}\,2\}$ | $86^\circ\ \langle 1\,\bar{2}\,1\,0\rangle$ |
| $\{1\,0\,\bar{1}\,1\}$ | $56^\circ\ \langle 1\,\bar{2}\,1\,0\rangle$ |
| $\{1\,0\,\bar{1}\,3\}$ | $64^\circ\ \langle 1\,\bar{2}\,1\,0\rangle$ |
| $\{1\,0\,\bar{1}\,1\}$ $\{1\,0\,\bar{1}\,2\}$ double twin | $38^\circ\ \langle 1\,\bar{2}\,1\,0\rangle$ |
| $\{1\,0\,\bar{1}\,3\}$ $\{1\,0\,\bar{1}\,2\}$ double twin | $22^\circ\ \langle 1\,\bar{2}\,1\,0\rangle$ |
| $\{1\,0\,\bar{1}\,2\}$ variant intersection 1 | $7^\circ\ \langle 1\,\bar{2}\,1\,0\rangle$ |
| $\{1\,0\,\bar{1}\,2\}$ variant intersection 2 | $60^\circ\ \langle 1\,0\,\bar{1}\,0\rangle$ |
| $\{1\,0\,\bar{1}\,2\}$ variant intersection 3 | $60^\circ\ \langle 8\,\bar{1}\,\bar{7}\,0\rangle$ |

is calculated as $\theta \pm (\alpha_{twin} - \alpha_{mat}) = 14.4^\circ \pm (19.29 + 3.42)^\circ = 37.11^\circ$. Based on the twin misorientation (Table 5 [47]), the twin in the Mg–Li–Zn is a $\{1\,0\,\bar{1}\,1\}$ $\{1\,0\,\bar{1}\,2\}$ double twin.

*AZ31*: The TEM image in Fig. 8 shows the twin structure of AZ31 alloy rolled 15 passes at 150 °C. A large number of parallel twins lying close to each other can be seen in the deformed microstructure of the AZ31 sample. Fig. 9 shows the TEM image of an AZ31 twin and the diffraction patterns from the twin and the matrix. The rotation angles of the matrix and the twin in the specimen during imaging of the diffraction patterns were $\alpha_{mat} = -4.24$, $\beta_{mat} = -3.43$ and $\alpha_{twin} = -5.22$, $\beta_{mat} = -6.77$. It could be seen that the differences between rotation angles of matrix and twins are $\Delta\alpha = 1$ and $\Delta\beta = 2.5$. Based on the diffraction patterns, the planes corresponding to these zones are $P_{Mat} = (0\,0\,0\,1)$ and $P_{twin} = (1\,0\,\bar{1}\,0)$ for the matrix and twin, respectively. The two planes make a 90° angle, thus, the twin misorientation is $90 \pm (\Delta\alpha + \Delta\beta) = 86.5^\circ$. Hence, the twin shown in Fig. 9 is a $\{1\,0\,\bar{1}\,2\}$ tensile twin (Table 5).

The difference between the edge cracking of the Mg–Zn–Li alloy and AZ31 can be explained in terms of the differences in their twinning behavior. It has been observed that subsequent slip-twin interactions largely determine the ductility of the HCP metals that undergo twinning [43]. If the twin boundaries become sinks for gliding dislocations the metal is ductile, if however, the dislocations are repelled by the twin boundary they pile-up at the interface leading to eventual crack nucleation. In Mg, the basal dislocations are repelled by $\{1\,0\,\bar{1}\,2\}$ tension twins [43] leading to cracking. This agrees well with the TEM analysis that shows profuse tension twinning in AZ31 which exhibits severe edge cracking.

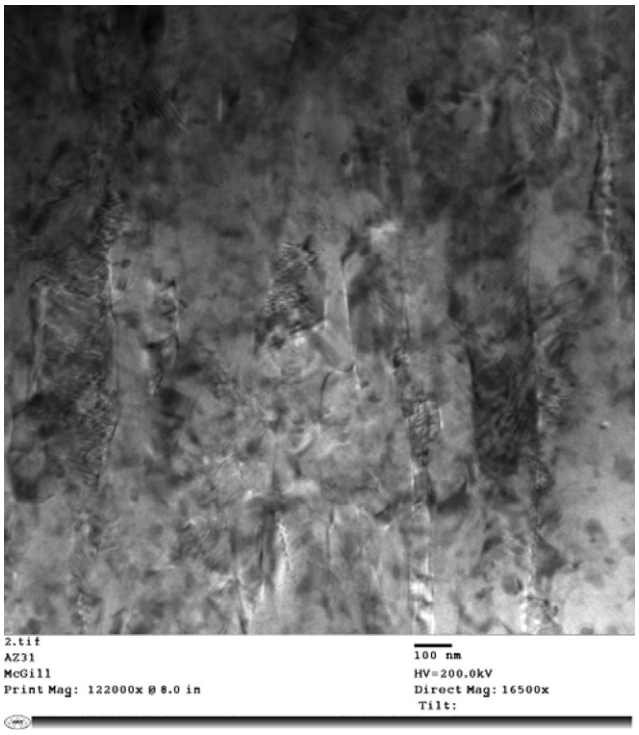


**Fig. 8.** TEM image of rolled AZ31 (15 passes at 150 °C) showing a large number of twins very close to each other.

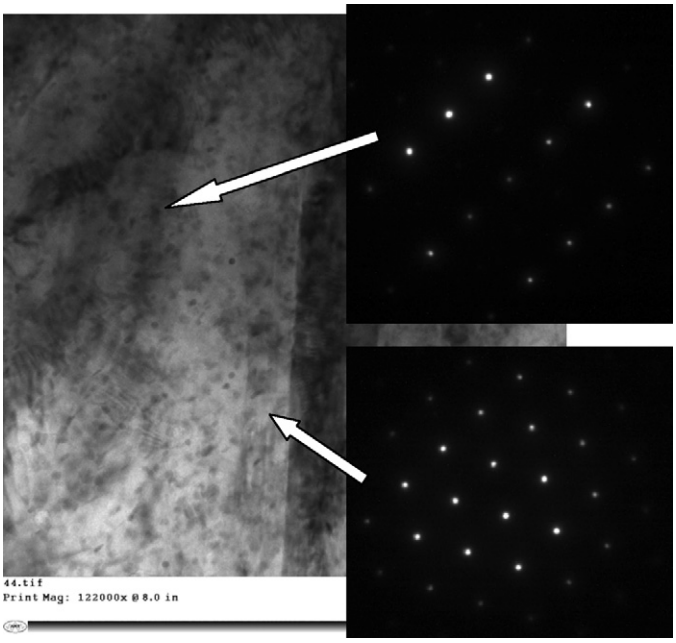


**Fig. 9.** The TEM image of a twin in AZ31 after 15 passes of rolling at 150 °C.

It is also interesting to note that the twinning can also be related to the axial ratio (Fig. 2). It is known that the twinning modes in HCP metals has been altered via alloying [43] that changes the axial ratio; e.g., twinning has been stopped in Mg–Cd alloy with $c/a = \sqrt{3}$, leading to extreme brittleness. With the aid of Fig. 2, it can be seen that while pure Mg with $c/a = 1.6240$ would exhibit the usual $\{1\,0\,\bar{1}\,2\}$ tension twins. The Li containing alloys in this study have $c/a = 1.619$ and in Fig. 2, move left towards Re ($c/a = 1.615$) which exhibits high ductility via profuse tension as well as compression twinning [43]. AZ31 has slightly higher $c/a$ than pure Mg, but the change is very small, only 0.04%, and in the opposite direction compared to the significant change in Li-containing alloys (0.3% change in $c/a$). Even so, AZ31 demonstrates slightly worse behavior than pure Mg with respect to edge cracking, indicating that even the slight increase in $c/a$, moving the alloy to the right of pure Mg in Fig. 2 adversely affects twinning related brittleness; at the $c/a$ of 1.6247, the shears of $\{1\,0\,\bar{1}\,2\}$ tension twins and $\{1\,0\,\bar{1}\,1\}$ compression twins start to differ making the atomic reshuffling more difficult during double twinning of AZ31 (i.e. double twinning is made difficult), leaving a higher propensity of tension twins which are potent sites for crack nucleation.

In this study it is observed that all alloys including AZ31 exhibit crack-free behavior up to 7 rolling passes (0.3 strain). Twinning is avoided because there are alternate deformation mechanisms, namely plastic-compatibility dependent non-basal slip at the grain boundaries. Beyond 7 rolling passes, the plastic compatibility is not solely sufficient to accommodate the additional strain in AZ31 and twinning sets in leading to edge cracking. Upon further strain the rolling behavior of AZ31 and the experimental alloys differ. In the experimental alloys, compression banding during rolling is prevented and rolling without major edge cracking is observed even at 15 passes (0.55 strain), which can be explained via changes in $c/a$ which affect twinning. Hence, it is understood that the important influence of axial ratio in edge cracking is through its effect on the twinning mode of the alloys.

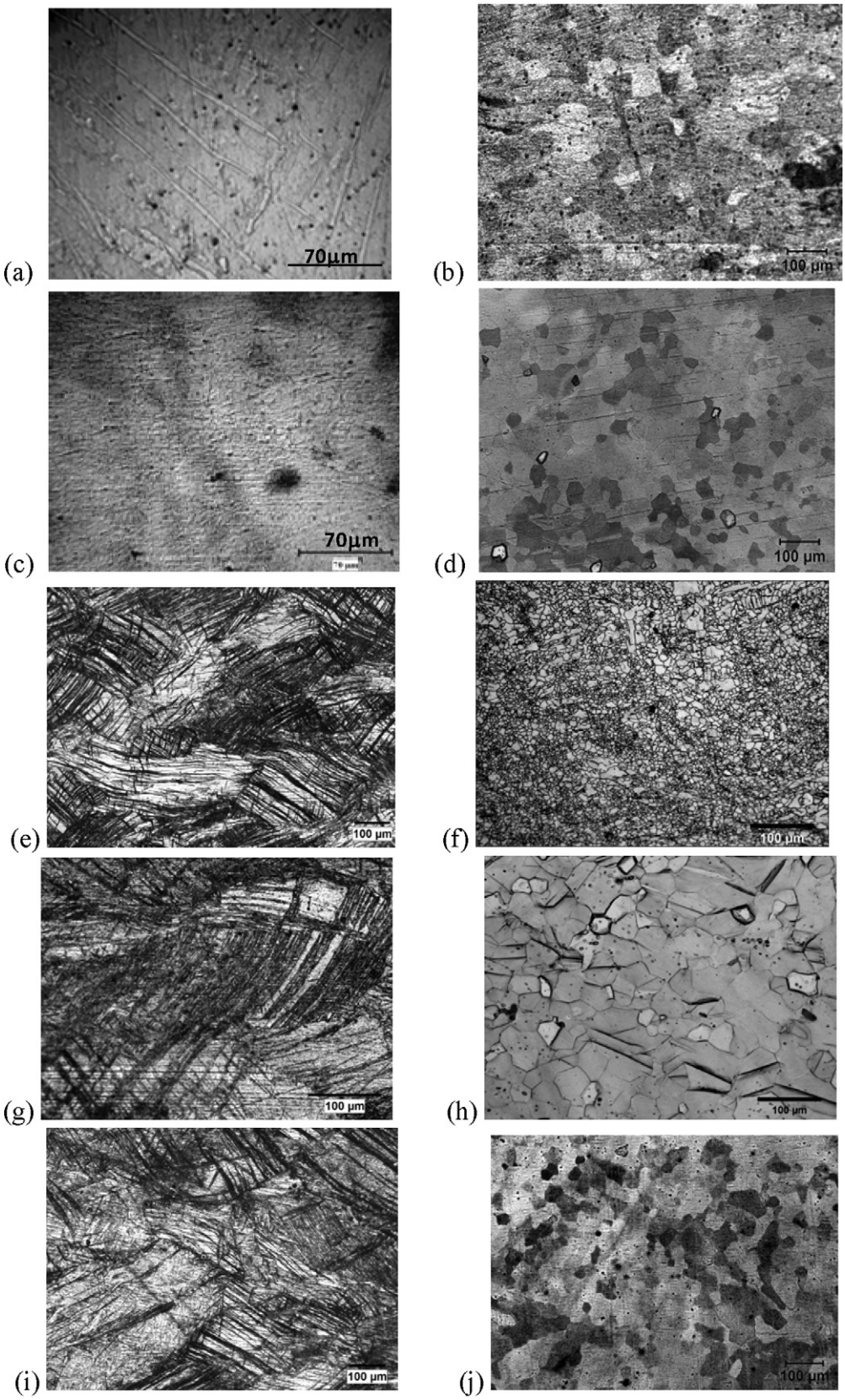


**Fig. 10.** Microstructures of (a and b) rolled and rolled/annealed Mg, (c and d) rolled and rolled/annealed Mg–1Zn–1In, (e and f) rolled and rolled/annealed AZ31, (g and h) rolled and rolled/annealed Mg–1Zn–2Li, and (i and j) rolled and rolled/annealed Mg–1Zn–2Li–1In.

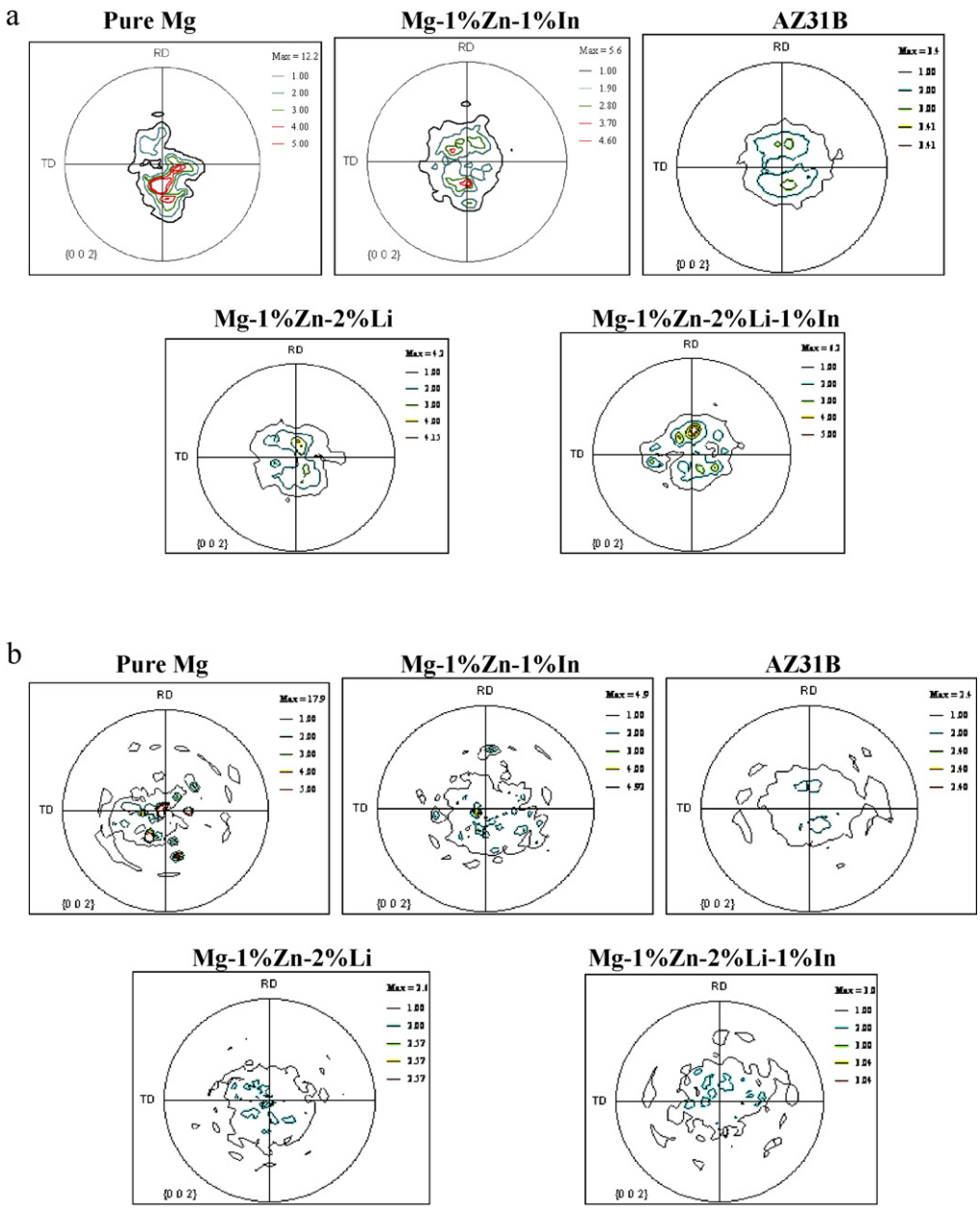


**Fig. 11.** (a) Pole figures showing the texture in rolled alloy specimens. (b) Texture (pole figures) of rolled and subsequently annealed alloy specimens.

## 5. Microstructures of rolled and annealed alloys

The microstructures of the alloys in the rolled and rolled/annealed conditions are shown in Fig. 10. Pure Mg exhibits a twinned structure typical of a moderate-temperature deformation. Annealing generates a recrystallized structure with an average grain size of 46 μm (Fig. 10a and b). AZ31 exhibits a bi-modal grain structure in the annealed condition (Fig. 10f). All other alloys are heavily deformed in the rolled condition and are recrystallized to an average grain size of 40–50 μm when annealed (Fig. 10b, c and g–j).

## 6. Texture of rolled and rolled/annealed alloys

The XRD results show that the specimens rolled at 150 °C have basal texture typical of 'rolling deformation texture' (Fig. 11a). The annealed specimens have recrystallized during 10 min at 400 °C; they, therefore, have a 'recrystallization texture' (Fig. 11b). However, the maximum intensity of the texture shows some variation. In the rolled samples, the maximum intensity, $M$, drops from 12 in pure Mg to 3.4 in AZ31. In the rolled/annealed samples, $M$ decreases from 17.9 (in Mg) to 2.4–2.6 (in AZ31 and Mg–2Li–1Zn) as seen in Table 4. Annealing decreases the maximum intensity in the texture of all alloys, while pure Mg shows a reverse trend: here, the maximum intensity increases from 12 to 18 upon annealing, which may be related to the recrystallization inside twinned regions or to the selection of grains with basal textures [48] during growth which would occur more easily in pure Mg with no solutes or precipitates.

The maximum intensity, $M$, in both rolling and in annealing textures correlates very well with the effective grain size in the as-cast condition (Fig. 12a and b), as

$$M_R = 1.4D' + 3 \quad \text{with} \quad R^2 = 0.88, \tag{7}$$

and

$$M_A = 2e^{-(D'/3)} \quad \text{with} \quad R^2 = 0.94. \tag{8}$$

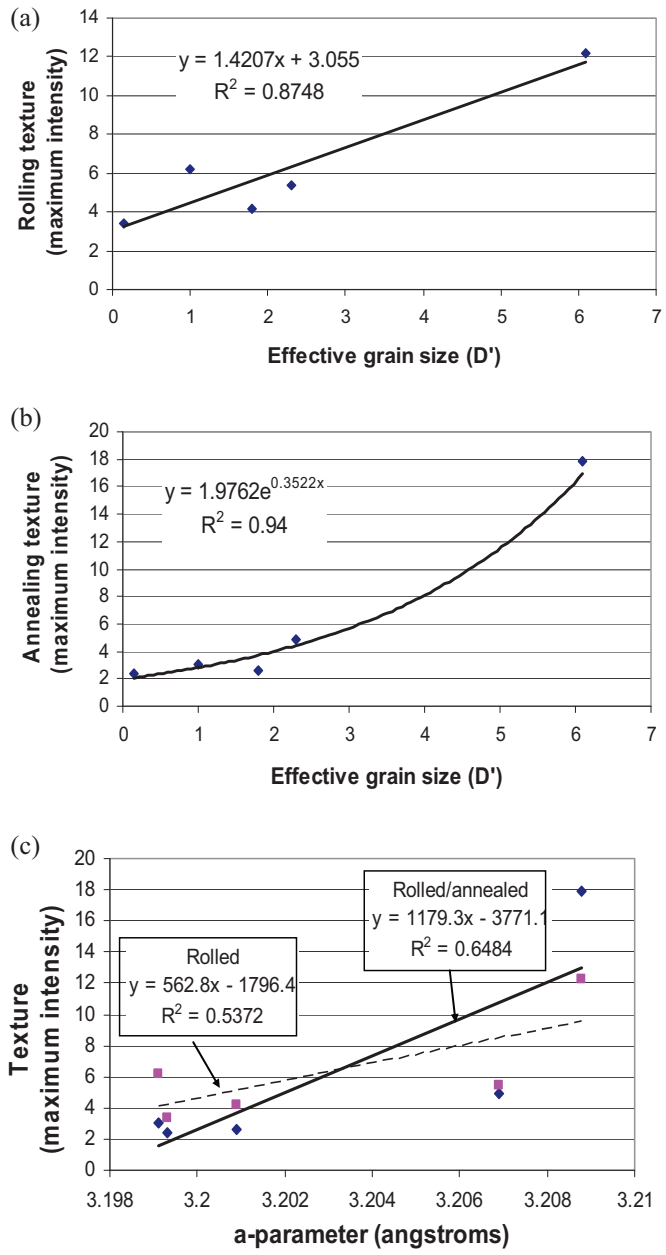


**Fig. 12.** The dependence of texture intensity on (a and b) the effective grain size, $D'$, and (c) on the $a$-parameter.

It agrees with previous observations [37] that a small grain size is needed to weaken texture through plastic compatibility [14]. As the grain size decreases, the amount of the non-basal slip-activity at the grain boundaries due to plastic compatibility stresses increases, and basal plane rotation perpendicular to the ND which occurs under the action of basal-slip becomes less dominant. This prevents the development of a strong basal texture in the rolled condition at 150 °C. To be noted that the maximum recrystallization texture intensity has an exponential relationship on the effective as-cast grain size. There is significant effect on texture strength in going from a large grain size of 6 mm down to 2–1 mm, but further weakening in texture necessitates large decreases in the initial grain size. This is the reason why processes such as ECAE that can produce initial grain sizes of 5–20 μm are effective in significantly weakening the texture in Mg alloys. Since grain size decreases within the 1000–100 μm range exert a small effect on texture intensity (from 3 to 2), most researchers do not report the observations on the effect of grain size on texture for conventionally cast alloys that are deformed.

There is no correlation, however, between axial ratio ($c/a$) and texture intensity and only a weak correlation with the $a$-parameter and texture intensity (Fig. 12c). This probably means that the decrease in $c/a$ ratios of the alloys studied is not sufficiently to activate substantial non-basal slip in the alloy at 150 °C to sufficiently lower the texture strength; however, it is effective in preventing twinning during rolling. A decrease in $a$ may have an influence in facilitating cross-slip of the partial dislocations [5] at the grain boundaries, thereby, contributing to texture weakening, as explained above, by reducing basal pole rotation stemming from extensive basal slip. Since the effect of $a$ is experienced mainly through cross-slip at the grain boundaries (due to the high local compatibility stresses there), its correlation to the overall texture intensity is also weak ($R^2 \sim 0.6$).

### 6.1. AZ31 alloy texture

The AZ31 alloy exhibits a basal texture with the lowest maximum intensity in both the rolled condition and after subsequent annealing. The lowest maximum intensity in texture seems to be associated with the AZ31 alloy, mainly due to the fine effective grain size and the slightly reduced $a$-parameter, which allow for plastic compatibility stresses to affect cross slip of partial dislocations. Grain size-dependent plastic compatibility provides an alternative deformation mechanism to basal slip and twinning until approximately 0.3 strain, reducing the strong basal texture. However, further straining cannot be accommodated solely by basal slip and plastic cross slip at grain boundaries and another deformation mechanism becomes necessary. The only other deformation mechanism at 150 °C is compression twinning and banding. The edge cracking becomes prominent at high strain (15 rolling passes rather than at 7 rolling passes), which can be explained by the onset of twinning in AZ31 at high strain [14] as a strain accommodation mechanism. It is interesting to note that the necklaced recystallization-structure of AZ31 in the annealed condition can be due to the local concentration of extensive deformation at grain boundaries due to its fine grain size (and large grain boundary area). Subsequent annealing leads to recrystallization at regions of high strain at the grain boundaries. The texture further weakens slightly as a result of sub-grain rotation during recrystallization.

### 6.2. The texture of experimental alloys with low axial ratio

The experimental alloys of this study all have Zn and Li and/or In in solid solution. The overall texture of these alloys, evolved during rolling and subsequent annealing, does not seemingly provide significant advantage over the AZ31 alloy. Mg–Zn–Li ternary alloy has the same texture intensity as AZ31; indium seems to very slightly strengthen texture in both ternary Mg–Zn–In and in the quaternary Mg–Zn–Li–In alloy compared to AZ31 and Mg–Zn–Li. The textures are weaker than pure Mg due to finer grain size but the grains are not as small as AZ31 to be able to give weaker textures than AZ31. The main advantage of the experimental alloys investigated in this study is the ability to influence twinning behavior due to lower $c/a$, which prevents twinning-related edge cracking at high strain; as a consequence these alloys show crack-free rolling. Mg–1Zn–2Li has the lowest texture intensity (similar to AZ31) but also exhibits minimum edge cracking, due to relatively fine grain size, low $c/a$ and $a$. Here, the difference in edge cracking in fine-grained experimental alloys and AZ31 is the $c/a$ ratio; low $c/a$ of 1.619 in the experimental alloys increases twinning related ductility at increased strain.

## 7. Synopsis

### 7.1. As-cast grain size

The rolling of the alloys at 150 °C indicated that effective grain size, if not accompanied by a low axial ratio ($c/a \sim 1.62$), does not play an important role in edge cracking at high strain. AZ31 with the smallest grain size but high $c/a$ exhibits the worst rolling behavior with severe edge cracks for $\varepsilon > 0.3$. All the alloys studied exhibit basal textures when rolled at 150 °C to 0.3 strain and after subsequent annealing. The texture intensity correlates with the effective as-cast grain size. The AZ31 alloy with the smallest grain size attains the weakest texture intensity both after rolling and after annealing. This can be attributed to plastic compatibility stresses leading to higher non-basal activity at the grain boundaries [14]. As discussed by Staroselsky and Anand [49], "in polycrystalline magnesium alloys, plastic deformation originates from both intragranular slip and twinning modes of deformation, as well as some intergranular deformation modes", the most important being grain boundary sliding. In their modeling of AZ31 deformation behavior, in order to account for the grain boundary deformation to match their stress–strain curves, the authors have used an approximate approach by adding a weighted isotropic term to the flow rule for grain boundary deformation which in their analysis was considered not to affect texture. This study reveals that grain size does have influence on texture pointing towards the importance of grain boundary deformation on texture evolution, however, as is expected large differences in grain size are needed to affect large differences in texture strength.

### 7.2. Lattice parameters and axial ratio

Edge cracking does show inverse relationship to axial ratio. The lowest edge cracking was observed for lithium-containing alloys with the lowest axial ($c/a$) ratio of 1.619 which is close to that of Re ($c/a = 1.615$) that shows twin-related high ductility (Fig. 2). This $c/a$ corresponds to an electron/atom ratio ($e/a$) of 1.9381 [23]. It is possible to develop other alloy compositions with similar $e/a$ and with potentially low edge cracking during rolling. Previous study [23] indicated that an electron/atom ratio ($e/a$) of ~1.83 and 2.03 would give an axial ratio of 1.58, similar to Ti which is known to have non-basal slip activation at room temperature. This study reveals the importance of $c/a$ on twinning behavior, wherein a $c/a$ of 1.62 becomes desirable. The $e/a$ ratio corresponding to that axial ratio would be ~1.93.

This study also underlines the importance of the as-cast grain size on texture development. The effective grain size evaluated in this study factors in both the grain size in the columnar grains region as well as in the equiaxed grain region. As such it gives a good indication of the grain structure of twin roll casting where a significant portion of the grain structure is columnar.

The results of this study confirm the importance of both the axial ratio ($c/a$) and the as-cast effective grain size (and structure) on having a magnesium sheet alloy that can exhibit low edge cracking at moderate temperatures and at the same time yield weak textures. To this end, solutes such as Li that can decrease $c/a$ of Mg to ~1.62 should be used in conjunction with solutes such as Zn that can produce grain refining. Indeed, Mg–2 wt%Li–1 wt%Zn alloy has shown the optimum combination of low edge cracking during rolling and a weak texture with potential advantages for working and forming. The decrease in the $a$-parameter may be additionally beneficial in facilitating the cross slip of partial dislocations at the grain boundaries and, thereby, contribute slightly to texture weakening both in the as-rolled and annealed conditions.

## Acknowledgements

The authors gratefully acknowledge the financial support of Natural Sciences and Engineering Research Council (NSERC) of Canada, General Motors of Canada and McGill University and thank Pierre Vermette for his valuable help in the casting experiments and Jay Tana of McGill University in optical microscopy and in texture measurements. Thanks are due to M. Masoumi for supporting microstructural and texture analysis.

## References

[1] E. Doege, K. Droder, J. Mater. Process. Technol. 115 (2001) 14–19.
[2] J.W. Christian, S. Mohajan, Prog. Mater. Sci. 39 (1995) 1–157.
[3] M.M. Myshlyaev, H.J. McQueen, A. Mwembela, E. Konopleva, Mater. Sci. Eng. A337 (2002) 121–133.
[4] S.I. Couling, J.F. Pashak, L. Sturkey, Trans. ASM 51 (1959) 94–107.
[5] T. Uesugi, M. Kohyama, M. Kohzu, K. Higasi, Mater. Sci. Forum, vols. 419–422, Trans. Tech., Switzerland, 2003, pp. 225–230.
[6] J. Koike, Mater. Sci. Forum, vols. 419–422, Trans. Tech., Switzerland, 2003, pp. 189–194.
[7] R. Ohyama, J. Koike, T. Kobayashi, M. Suzuki, K. Maruyama, Mater. Sci. Forum, vols. 419–422, Trans. Tech., Switzerland, 2003, pp. 237–242.
[8] S.E. Ion, F.J. Humphreys, S.H. White, Acta Metall. 30 (1982) 1909–1919.
[9] A. Grosvenor, C.H.J. Davies, Mater. Sci. Forum 426–432 (2003) 4567.
[10] Y. Yoshida, L. Cisar, S. Kamado, J. Koike, Y. Kojima, Mater. Sci. Forum (2003) 533–538.
[11] L. Cisar, Y. Yoshida, S. Kamado, Y. Kojima, Mater. Sci. Forum (2003) 249–254.
[12] W.J. Kim, H.G. Jeong, Mater. Sci. Forum (2003) 201–206.
[13] Y. Miyahara, K. Matsubara, K. Neishi, Mater. Sci. Forum (2003) 551–556.
[14] J. Koike, T. Kobayashi, T. Mukai, H. Watanabe, M. Suzuki, K. Maruyama, K. Higashi, Acta Mater. 51 (2003) 2055–2065.
[15] M. Masoumi, F. Zarandi, M. Pekguleryuz, Scripta Mater. 62 (11) (2010) 823–826.
[16] M. Masoumi, F. Zarandi, M. Pekguleryuz, Mater. Sci. Eng. A 528 (2011) 1268–1279.
[17] L.W.F. Mackenzie, M.O. Pekguleryuz, Scripta Mater. 59 (6) (2008) 665–668.
[18] L.W.F. Mackenzie, M. Pekguleryuz, Mater. Sci. Eng. A 480 (2008) 189–197.
[19] H. Yana, R.S. Chena, E.H. Han, Mater. Sci. Eng. A 527 (2010) 3317–3322.
[20] L. Li, X. Zhang, C. Tanga, Y. Denga, N. Zhou, Mater. Sci. Eng. A 527 (2010) 1266–1274.
[21] H.K. Lim, D.H. Kima, J.Y. Lee, W.T. Kim, D.H. Kim, J. Alloys Compd. 468 (2009) 308–314.
[22] M. Masoumi, M. Hoseini, M. Pekguleryuz, Mater. Sci. Eng. A A528 (2011) 3122–3129.
[23] A. Becerra, M. Pekguleryuz, J. Mater. Res. 23 (12) (2008) 3379–3386.
[24] A. Becerra, M. Pekguleryuz, J. Mater. Res. 24 (5) (2009) 1722–1729.
[25] H.J. McQueen, M.O. Pekguleryuz, in: B.L. Mordike, F. Hehmann (Eds.), Magnesium Alloys and their Applications, DGM, 1992, pp. 101–108.
[26] Hot Working Guide, in: Y.V.R.K. Prasad, S. Sasidhara (Eds.), A Compendium of Processing Maps, ASM, 1997, pp. 343–381.
[27] E.F. Emley, Principles of Magnesium Technology, Pergamon Press, London, 1966.
[28] G.V. Raynor, The Physical Metallurgy of Magnesium and its Alloys, Pergamon Press, New York, 1959.
[29] J.F. Stohr, J.P. Poirier, Phil. Mag. 25 (1972) 1313–1329.
[30] S.R. Agnew, M.H. Yoo, C.N. Tome, Acta Mater. 49 (2001) 4277–4289.
[31] S.R. Agnew, J.A. Horton, M.H. Yoo, Metall. Mater. Trans. 33A (2002) 851–858.
[32] M.A. Meyers, O. Vohringer, V.A. Lubarda, Acta Mater. 49 (2001) 4025.
[33] A. Yamashita, Z. Horita, T.G. Langdon, Mater. Sci. Eng. A 300 (2001) 142.
[34] H. Margolin, M.S. Stanescu, Acta Metall. 23 (1975) 1411.
[35] T. Quested, Solidification of Inoculated Aluminum Alloys, PhD thesis, Univ. Cambridge, 2004.
[36] F. Kaiser, D. Letzig, J. Bohlen, A. Styczynski, Ch. Hartig, K.U. Kainer, in: K.U. Kainer (Ed.), Magnesium Alloys and their Applications, DGM, Wiley-VCH, Germany, 2000, pp. 315–320.
[37] M.R. Barnett, Mater. Sci. Forum, vols. 419–422, Trans. Tech., Switzerland, 2011, pp. 503–508.
[38] L.W.F. Mackenzie, B. Davis, F.J. Humphreys, G.W. Lorimer, Mater. Sci. Technol. 23 (10) (2007) 1173–1180.
[39] E. Ball, P. Prangnell, Scripta Metall. Mater. 31 (1994) 111–116.
[40] J.W. Senn, S.R. Agnew, in: M.O. Pekguleryuz, L.W.F. Mackenzie (Eds.), Proc. Magnesium Technology in the Global Age, Montreal, Canada, October 1–4, 2006, p. 115.
[41] G. Sambasiva, Y.V.R.K. Prasad, Mater. Lett. 1 (5, 6) (1983) 171–174.
[42] H. Yoshinaga, T. Obara, S. Morozumi, Mater. Sci. Eng. 12 (1973) 255–264.
[43] M.H. Yoo, Metall. Trans. A 12A (1981) 409–418.
[44] M.H. Yoo, J.K. Lee, Phil. Mag. A 63 (5) (1991) 987–1000.
[45] J. Wang, J.P. Hirth, C.N. Tome, Acta Mater. 57 (2009) 5521–5530.
[46] D.W. Hogan, D.J. Dyson, Micron 2 (1970) 59–61 (1969).
[47] N. Stanford, Phil. Mag. Lett. 88 (2008) 379–386.
[48] K. Hantzsche, J. Bohlen, J. Wendt, K.U. Kainer, S.B. Yi, D. Letzig, Scripta Mater. 63 (2010) 725–730.
[49] A. Staroselsky, L. Anand, Int. J. Plastic. 19 (2003) 1843–1864.